Computers & Geosciences 51 (2013) 247–254

Contents lists available at SciVerse ScienceDirect

Computers & Geosciences

journal homepage: www.elsevier.com/locate/cageo

# Preferential filtering for gravity anomaly separation

Lianghui Guo [a,b,*], Xiaohong Meng [a,b], Zhaoxi Chen [a,b], Shuling Li [a,b], Yuanman Zheng [a,b]

[a] School of Geophysics and Information Technology, China University of Geosciences (Beijing), Beijing 100083, China
[b] Key Laboratory of Geo-detection (China University of Geosciences, Beijing), Ministry of Education, Beijing 100083, China

ARTICLE INFO

*Article history:*
Received 4 July 2012
Received in revised form
2 September 2012
Accepted 4 September 2012
Available online 18 September 2012

*Keywords:*
Gravity anomaly
Separation
Regional-residual
Preferential filtering

ABSTRACT

We present the preferential filtering method for gravity anomaly separation based on Green equivalent-layer concept and Wiener filter. Compared to the conventional upward continuation and the preferential continuation, the preferential filtering method has the advantage of no requirement of continuation height. The method was tested both on the synthetic gravity data of a model of multiple rectangular prisms and on the real gravity data from a magnetite area in Jilin Province, China. The results show that the preferential filtering method produced better separation of gravity anomaly than both the conventional low-pass filtering and the upward continuation.



## 1. Introduction

The observed gravity anomalies are the sum of gravity effects of density differences at various depths in the subsurface half space. In order to study a specific geological problem using gravity data, the target anomalies must first be separated from the observed gravity anomalies. In the literature, there are a variety of methods proposed for separating gravity anomalies, such as upward continuation (Nettleton, 1954; Jacobsen, 1987), matched filtering (Spector and Grant, 1970), polynomial fitting (Telford et al., 1990), Wiener filtering (Pawlowski and Hansen, 1990), preferential continuation (Pawlowski, 1995), wavelet transformation multiple-scale decomposition (Fedi and Quarta, 1998) and nonlinear filtering (Keating and Pinet, 2011).

One of two key problems of the conventional upward continuation (Nettleton, 1954; Jacobsen, 1987) is that the shallow-source short-wavelength signals and deep-source long-wavelength signals are both simultaneously upward continued and consequently are both attenuated. After subtracting the upward continued regional signals from the observed anomalies, the resultant residual signals still contain parts of regional signals. It means that the anomaly separation is not complete. To solve this problem, Pawlowski (1995) proposed the preferential continuation method based on Green's equivalent layer concepts and Wiener filtering principle. This method attenuates shallow-source short-wavelength signals while minimally attenuating deep-source long-wavelength signals. Later, Xu and Zeng (2000) and Meng et al. (2009) suggested the algorithm of the difference continuation based on the preferential continuation. The algorithm is used to extract certain signals of a given wavelength band, similar to the conventional band-pass filtering.

Another problem of the conventional upward continuation, which also occurs in the preferential continuation (Pawlowski, 1995) and its difference continuation algorithm (Xu and Zeng, 2000; Meng et al., 2009), is that the continuation height must be known. To overcome this problem, Zeng et al. (2008) presented a practical algorithm, based on model studies, to derive an optimum continuation height by calculating a series of cross-correlations between the upward continuations at two successive heights. The average height of the maximum deflection of these cross-correlation values yields the optimum continuation height for regional-residual separation. Guo et al. (2009) and Meng et al. (2009) proposed a similar algorithm for estimating the optimum continuation height of the preferential upward continuation.

In this article we attempted to make a further study on this subject. We proposed the preferential filtering method based on Green's equivalent layer concepts and Wiener filterer. The method extracts certain signals of a given wavelength band without the requirement of upward continuation height.

We first presented the principle and procedure of the preferential filtering. Then we performed data experiments on both synthetic data and real gravity data respectively using the preferential filtering. The conventional low-pass filtering and the upward continuation methods were also used to test the data for comparisons.

* Corresponding author at: School of Geophysics and Information Technology, China University of Geosciences (Beijing), Beijing 100083, China.
Tel./fax: +86 1082 322 648.
*E-mail address:* guo_lianghui@163.com (L. Guo).

0098-3004/$ - see front matter © 2012 Elsevier Ltd. All rights reserved.
http://dx.doi.org/10.1016/j.cageo.2012.09.012

## 2. The principle of the preferential filtering

### 2.1. The preferential filtering operator

The observed gravity anomaly $g_{obs}(x,y)$ may often be regarded as the sum of the deep-source long-wavelength gravity anomaly $g_d(x,y)$ and the shallow-source short-wavelength gravity anomaly $g_s(x,y)$ such that

$$g_{obs}(x,y)=g_d(x,y)+g_s(x,y). \tag{1}$$

Then the power spectrum density function of the observed gravity anomaly $P$ may be regarded as the sum of the power spectrum density function of deep-source anomaly $P_d$ and that of shallow-source anomaly $P_s$ (Pawlowski, 1994),

$$P=P_d+P_s. \tag{2}$$

The Fourier power spectrum of the observed gravity anomaly may be modeled by invoking Green's equivalent-layer concept for the deep-source and shallow-source anomalies in Eq. (1) (Pawlowski, 1994). In practice, it is the easiest way to model the observed gravity anomaly's radially averaged logarithm power spectrum, which may be modeled with an appropriate $m+n$ number of equivalent source layers at various depths such that (Pawlowski, 1994)

$$P=P_{d_1}+P_{d_2}+\cdots+P_i+\cdots+P_{d_m}+P_{s_1}+P_{s_2}+\cdots+P_j+\cdots+P_{s_n}+E, \tag{3}$$

where the deep-source component is modeled with $m$ equivalent source layers, while the shallow-source component is modeled with $n$ equivalent source layers. Error $E$ arises from the inadequacy of the spectral model to perfectly fit the observed data's power spectrum.

Following Naidu (1968) and Dampney (1969), the power spectral density function for each equivalent source layer at depth $h$ from the observation datum (in Eq. (3)) may be defined as

$$P=se^{-2kh} \tag{4}$$

where $s$ is a constant term directly proportional to the expected equivalent source layer strength, and $k$ is the angular wave vector.

Suppose that the target is layers $i\to j$ $(n+m\geq j\geq i\geq 1)$ in the subsurface. The preferential filtering expects to keep the anomalies of target layers unchanged while the anomalies of the other layers are suppressed. Hence, the expected output is

$$g_{pf}(x,y)=g_{i\to j}(x,y). \tag{5}$$

Then, assume that the input of the Wiener filter is the observed anomaly $g_{obs}(x,y)$ and the expected output is $g_{pf}(x,y)$. The transfer function of the required Wiener filter (Wiener, 1949; Clarke, 1969) takes the form

$$W(f)=\frac{\langle G_{pf}G^*\rangle}{\langle GG^*\rangle}, \tag{6}$$

where, $G$ signifies spatial frequency (wavenumber) domain terms, the angle bracket pairs $\langle\ \rangle$ denotes the mathematical expectation and the asterisks $(^*)$ indicates the complex conjugation. The numerator of the equation is merely the cross-power spectrum density function of the filter input (the observed gravity anomaly) and the expected filter output, while the denominator is the power spectrum density function of the filter input.

Combined with Eq. (3), the transform function of the Wiener filter in Eq. (6) can be rewritten as

$$W_{pf}=\frac{P_{(i\to j)}+P'_{(i\to j)}}{P}, \tag{7}$$

where, $P_{(i\to j)}$ is the power spectrum density function of the anomalies of target layers, while $P'_{(i\to j)}$ is the cross-power spectrum density function of the anomalies of target layers and those of the other layers.

Assuming that the anomalies of the target layers are uncorrelated with those of the other layers, there is $P'_{(i\to j)}=0$. Thus the above transform function of the Wiener filter can be rewritten as

$$W_{\mathrm{pf}}=\frac{P_{(i\to j)}}{P}. \tag{8}$$

We call the above equation as the preferential filtering operator. When $i=1$, $i\to j$ means $i\to j$. In this case, the preferential filtering is a low-pass filtering that separates anomalies of $i\to j$ layers. When $j=m+n$, $i\to j$ means $i\to m+n$, then the preferential filtering is a high-pass filtering that separates anomalies of $i\to m+n$ layers. If $n+m>j\geq i>1$, the preferential filtering is a band-pass filtering that separates anomalies of $i\to j$ layers. Therefore, the preferential filtering plays different roles in separating anomalies by using Eq. (8), with the separated anomalies being the response of the target layers on the original observation surface.

### 2.2. The procedure of the preferential filtering

The procedure of the preferential filtering for separating anomalies is described as follows:

(1) Perform Fourier transformation to the observed gravity anomaly and then calculate the radial averaged logarithm power spectrum (see black line in Figs. 1 and 2).

(2) Fit the radially averaged logarithm power spectrum by using piece-wise linearization (see blue lines in Fig. 2).
First, analyze shape features of the radially averaged logarithm power spectrum and determine the number of sections for piece-wise linearization and their separated radial frequency ranges. The lower the radially frequencies are, the more narrow sections are segmented, and vice versa. Each section corresponds to each equivalent-source layer. Generally, low radial frequency sections mainly relate to regional deep layers, and intermediate radial frequency sections mostly correspond to shallow layers, while high radial frequency sections are dominated by noise (Spector and Grant, 1970; Pawlowski and Hansen, 1990; Pawlowski, 1994). The range of low radial frequency section is small while that of high one is large. Then, fit the radially averaged logarithm power spectrum in each section using a straight line. Finally, estimate the depth of each equivalent layer using the following equation (Spector and Grant, 1970; Boler, 1978; Connard et al., 1983)
$$h=\frac{P(r_1)-P(r_2)}{4\pi(r_2-r_1)} \tag{9}$$
where, $r_1$ and $r_2$ are respectively the start and end of radial frequencies of the fitted straight line, and $P(r_1)$ and $P(r_2)$ corresponds radially averaged logarithm power spectrum.

(3) Fit the radially averaged logarithm power spectrum by using the power spectrum density function models of Eq. (4) and the estimated depths of equivalent-source layers (see red line in Fig. 2).
Supposing $a=e^{-2kh}$, Eq. (4) has the following form for the $i$th radial frequency sample point,
$$P_i=a_{i,\,1}s_1+a_{i,\,2}s_2+\cdots+a_{i,\,m+n}s_{m+n}+e_i \tag{10}$$
where $P_i$ is the radially averaged logarithm power spectrum of the $i$th radial frequency sample point and $e_i$ is the error in fitting the spectral model of Eq. (4) to the $i$th radial frequency sample point. Error $e_i$ could arise, for instance, from an inadequacy in the spectral model to satisfy the observed gravity anomaly's power spectrum.

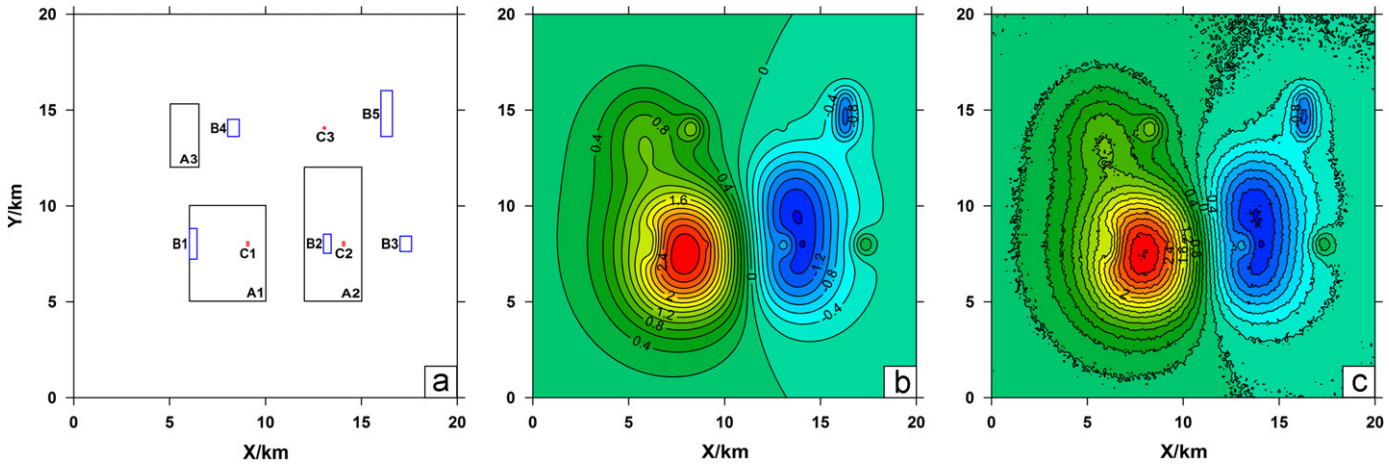


**Fig. 1.** The outline of the model on the horizontal plane (a), the theoretical gravity anomaly of the model (b), and the noised gravity anomaly (c). The unit of gravity anomaly is mGal.

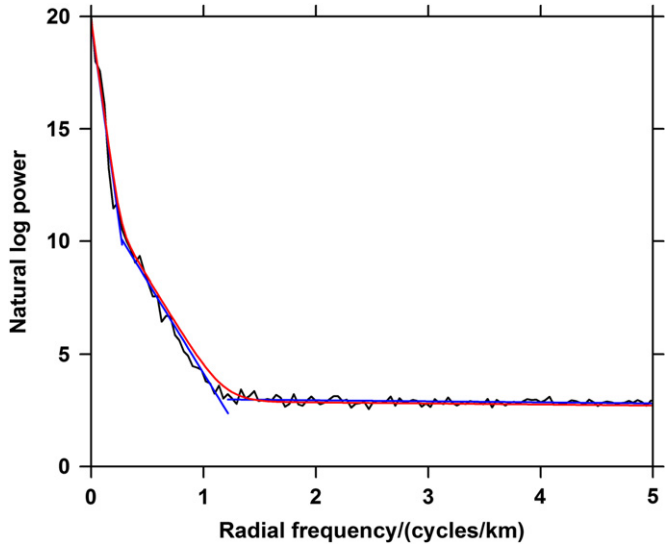


**Fig. 2.** The radially averaged logarithm power spectrum of the noised gravity anomaly (black line) and its fitting by using piece-wise linearization. The blue lines show the fitted straight lines in each radial frequency section, and the red line indicates the fitted radial logarithm power spectrum by using power spectrum density function models. (For interpretation of the references to color in this figure legend, the reader is referred to the web version of this article.)

For $l$ spectral samples, there is a system of $l$ linear equations written in matrix notation as

$$\begin{bmatrix} P_1 \\ P_2 \\ \vdots \\ P_l \end{bmatrix} = \begin{bmatrix} a_{1,1} & a_{1,2} & \cdots & a_{1,m+n} \\ a_{2,1} & a_{2,2} & \cdots & a_{2,m+n} \\ \vdots & \vdots & \ddots & \vdots \\ a_{l,1} & a_{l,2} & \cdots & a_{l,m+n} \end{bmatrix} \begin{bmatrix} s_1 \\ s_2 \\ \vdots \\ s_{m+n} \end{bmatrix} + \begin{bmatrix} e_1 \\ e_2 \\ \vdots \\ e_l \end{bmatrix}. \quad (11)$$

Eq. (11) can be rewritten with a more compact form as

$$\mathbf{P} = \mathbf{AS} + \mathbf{E}. \quad (12)$$

The least square solution of Eq. (12) is given by

$$\mathbf{S} = [\mathbf{A}^T\mathbf{A}]^{-1}\mathbf{A}^T\mathbf{P}. \quad (13)$$

Then by using an iterative optimization algorithm such as the conjugate gradient algorithm (Hestenes and Stiefel, 1952) or its analogs, Eq. (12) can be solved to obtain the vector **S**. Then using the vector **S** and Eq. (4), we can calculate the power spectrum either for the *i*th radial frequency sample point or for the ith equivalent-source layer.

(4) Construct the operator of preferential filtering according to Eq. (8).
(5) Apply the preferential filtering of Eq. (8) to the observed gravity anomaly.
(6) Reverse Fourier transform to yield the separated target anomalies in space domain.

## 3. Data experiments

### 3.1. Test on the synthetic data

The test model consists of eleven rectangular prisms with various sizes and density contrasts (Fig. 1a). The large prisms A1, A2 and A3 are in the deeper layer (layer A), the small prisms B1–B5 are in the middle layer (layer B), and the smallest prisms C1–C3 are in the shallower layer (layer C). We did forward modeling of the model for gravity anomaly on a flat surface with an elevation of 0 m. The observed geometry is a $201 \times 201$ regular grid with grid spacing of 0.1 km along both *X*-axis and *Y*-axis. Fig. 1b and c separately show the map of the theoretical gravity anomaly of the model and that was contaminated by Gaussian random noise of 4% of the datum magnitude.

We calculated the radially averaged logarithm power spectrum of the noised gravity anomaly and then fit it by using piece-wise linearization (Fig. 2). In this case, we separated the radial frequency of the power spectrum into three sections, 0–0.2745 cycles/km (frequency band 1), 0.2725–1.2157 cycles/km (frequency band 2) and 1.2157–5 cycles/km (frequency band 3). Theoretically, the power spectrum of frequency band 1 mainly corresponds to long-wavelength anomalies caused by the prisms of layer A, that of frequency band 2 to short-wavelength anomalies caused by the prisms of layers B and C, and that of frequency band 3 to high-frequency random noise.

Then we attempted to do different separations of the noised gravity anomaly by using the preferential filtering method. First, we used the method to remove the Gaussian noise, which played a role of low-pass filtering. Fig. 3a and d, respectively, displays the amplitude response to the preferential filtering operator and the denoised anomalies. The result shows that the Gaussian noise was suppressed effectively, and the anomalies of layers A and B were preserved well, though such a preservation for layer C was not very effective (because its frequency was close to that of noise).

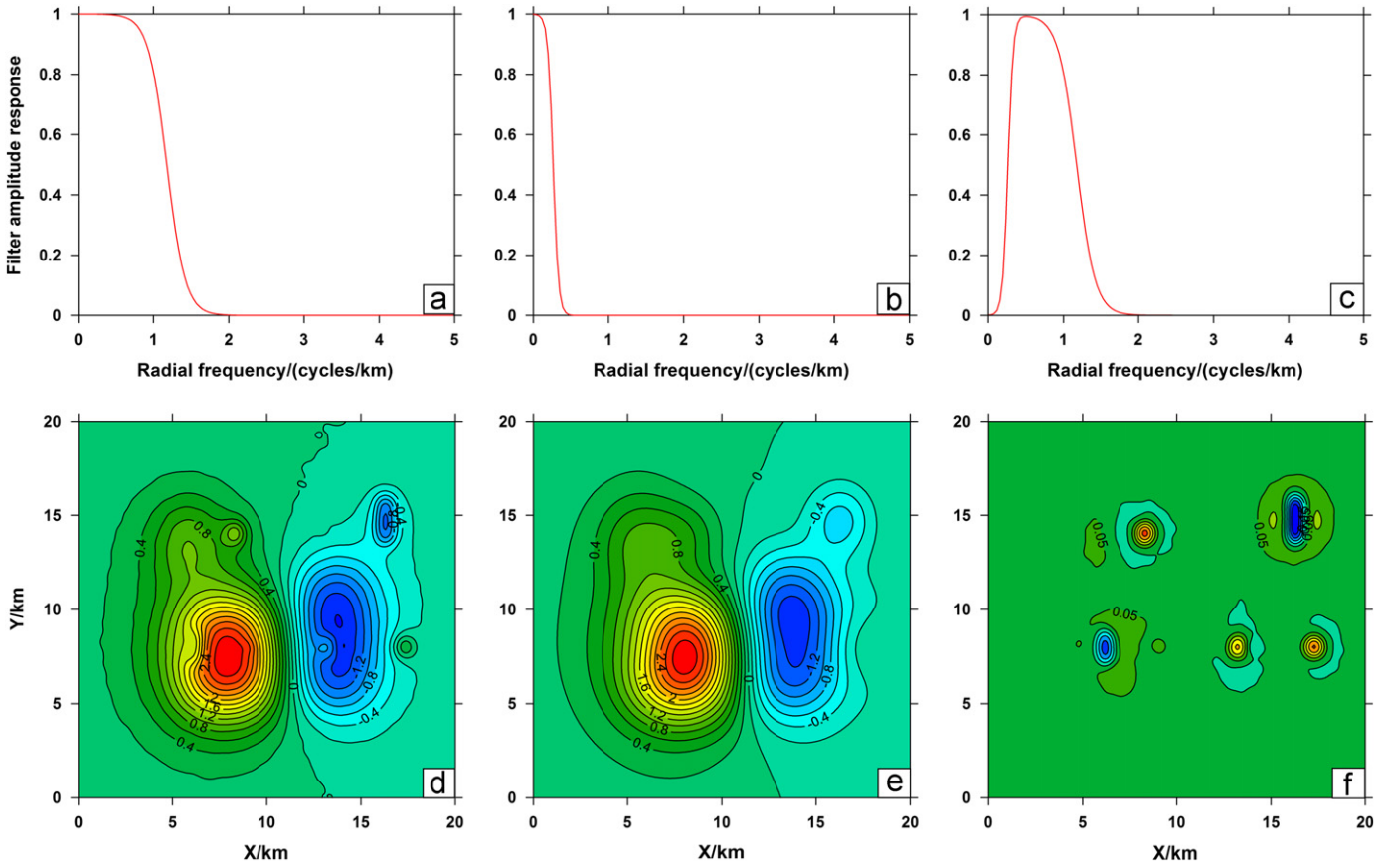


**Fig. 3.** The amplitude response of the preferential filtering operator for removing Gaussian noise (a), separating regional anomalies of layer A (b), and separating local anomalies of layers B and C (c). (d)–(f) shows the corresponding anomalies of (a)–(c). The unit of gravity anomaly is mGal.

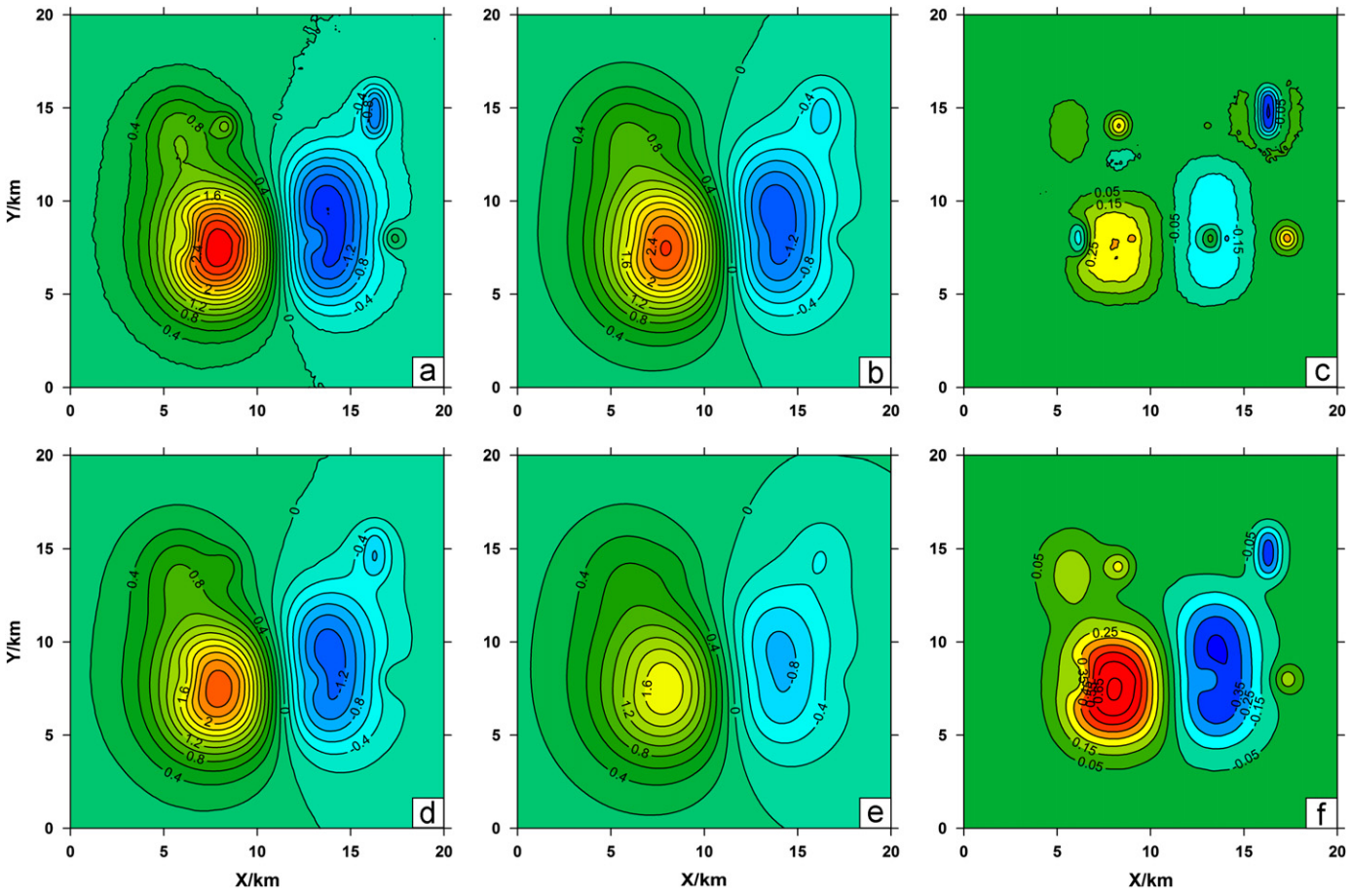


**Fig. 4.** The denoised anomalies (a), the separated regional anomalies (b) and the separated local anomalies (c) by using the low-pass filtering, and those (d–f) of the upward continuation. The unit of gravity anomaly is mGal.

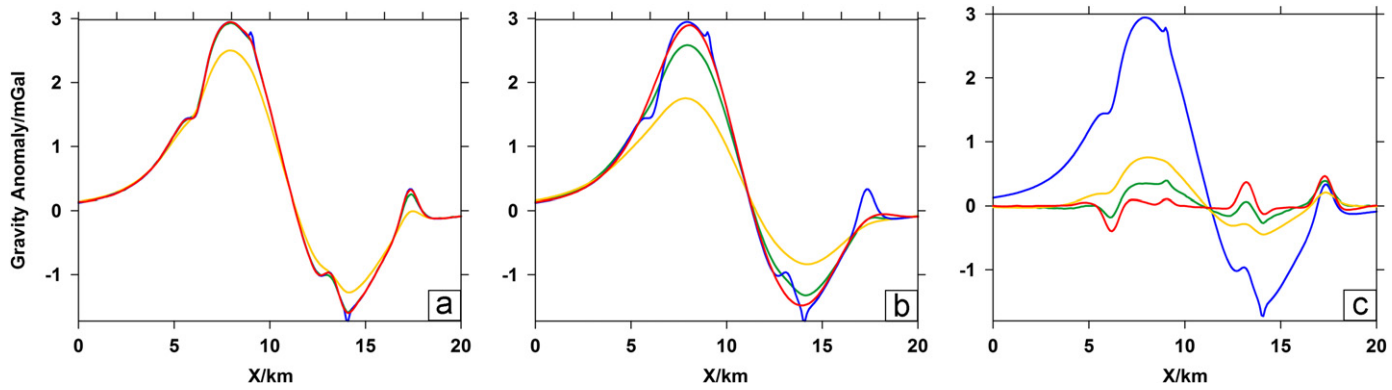


**Fig. 5.** Comparisons between the theoretical gravity anomaly (blue lines) and the separated anomalies by using the three methods along profile $X=5680$ m: (a) the denoised anomalies, (b) the separated regional anomalies, (c) the separated local anomalies. Red lines correspond to the preferential filtering, green lines to the low-pass filtering, and yellow lines to the upward continuation. (For interpretation of the references to color in this figure legend, the reader is referred to the web version of this article.)

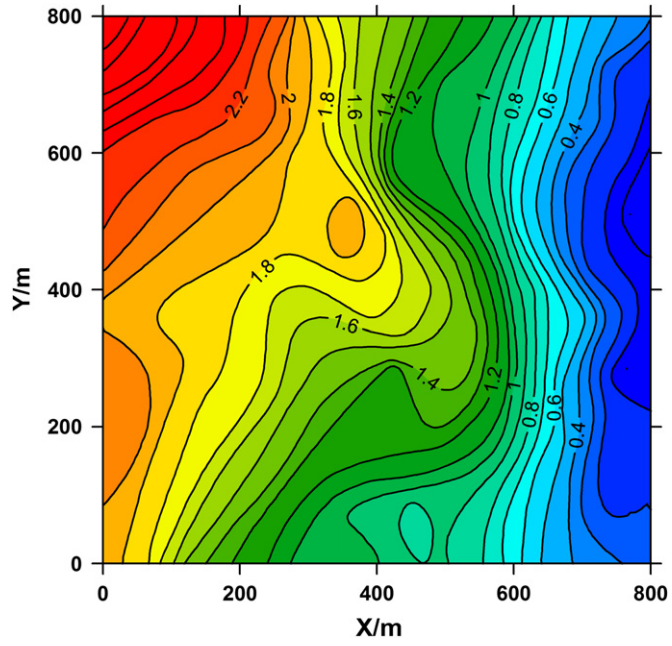


**Fig. 6.** The real Bouguer gravity anomaly from an iron deposit in Jilin Province. The unit of gravity anomaly is mGal.

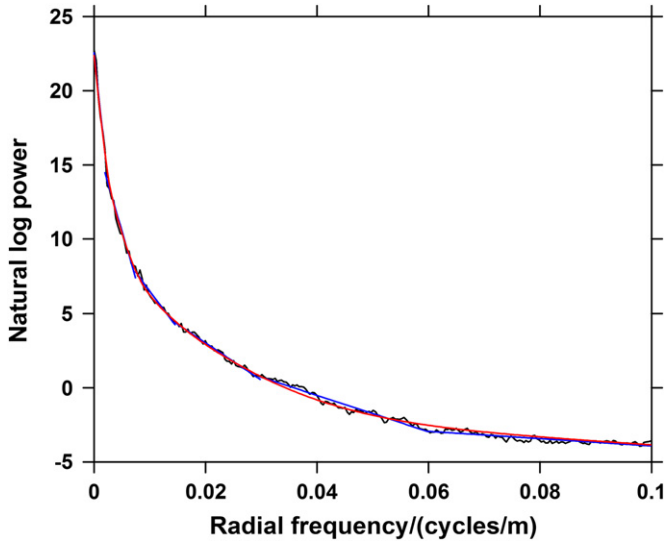


**Fig. 7.** The radially averaged logarithm power spectrum of the real Bouguer gravity anomaly (black line) and its fitting by using piece-wise linearization. The blue lines show the fitted straight lines in each radial frequency section, and the red line indicates the fitted radial logarithm power spectrum by using the power spectrum density function models. (For interpretation of the references to color in this figure legend, the reader is referred to the web version of this article.)

Next, we used the method to separate the regional anomalies of frequency band 1, which still played a role of low-pass filtering. Fig. 3b and e), respectively, shows the amplitude response to the preferential filtering operator and the separated anomalies. The result demonstrates that both the Gaussian noise and the local anomalies of layers B and C were effectively suppressed, while the anomalies of layer A were well preserved. Finally, we used the method to separate the local anomalies of frequency band 2, which played a role of band-pass filtering. Fig. 3c and f, respectively, shows the amplitude response to the preferential filtering operator and the separated anomalies. The result indicates that both the Gaussian noise and the regional anomalies of layer A were suppressed, while the local anomalies of layers B and C are well conserved.

For comparisons, we also performed the same data test by using the conventional low-pass filtering and the upward continuation, respectively. To remove the Gaussian noise, the cut-off wavelength of the low-pass filtering was chosen as 800 m, and the continuation height of the upward continuation was chosen as 300 m. To separate the regional anomalies of layer A, the cut-off wavelength of the low-pass filtering was chosen as 4000 m, and the upward continuation height was chosen as 1000 m. Fig. 4a and b, respectively, shows the denoised anomalies and the separated regional anomalies by the low-pass filtering. Fig. 4d and e displays those of the upward continuation. To separate the local anomalies of layers B and C, we subtracted the regional anomalies in Fig. 4b and e, respectively, from the denoised anomalies in Fig. 4a and c. The resultant local anomalies by both methods are shown in Fig. 4c and f, respectively. The results show that the Gaussian noise was attenuated effectively by both methods, while their regional-residual anomalies separation was not complete. The local anomalies (Fig. 4c) separated by the low-pass filtering remained partially regional anomalies, and those (Fig. 4f) of the upward continuation contained more regional anomalies.

Fig. 5 showed comparisons between the theoretical gravity anomaly (no noise) and the separated anomalies by using the preferential filtering, the low-pass filtering and the upward continuation along profile $X=5680$ m. The denoised anomalies (Fig. 5) of the three methods were roughly consistent, while

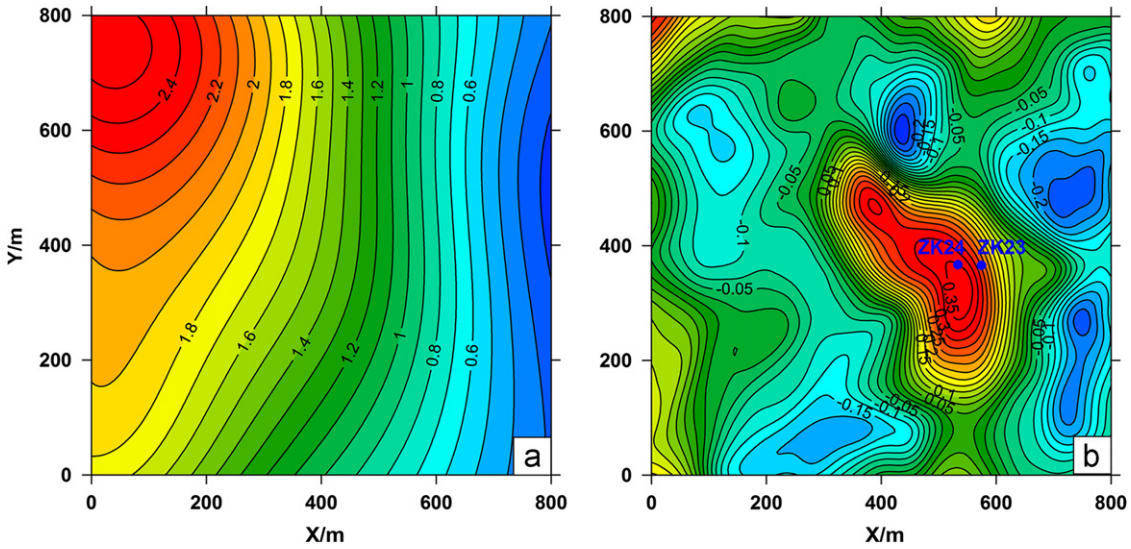


**Fig. 8.** The regional anomalies (a) and the local anomalies (b) separated by the preferential filtering. The unit of gravity anomaly is mGal.

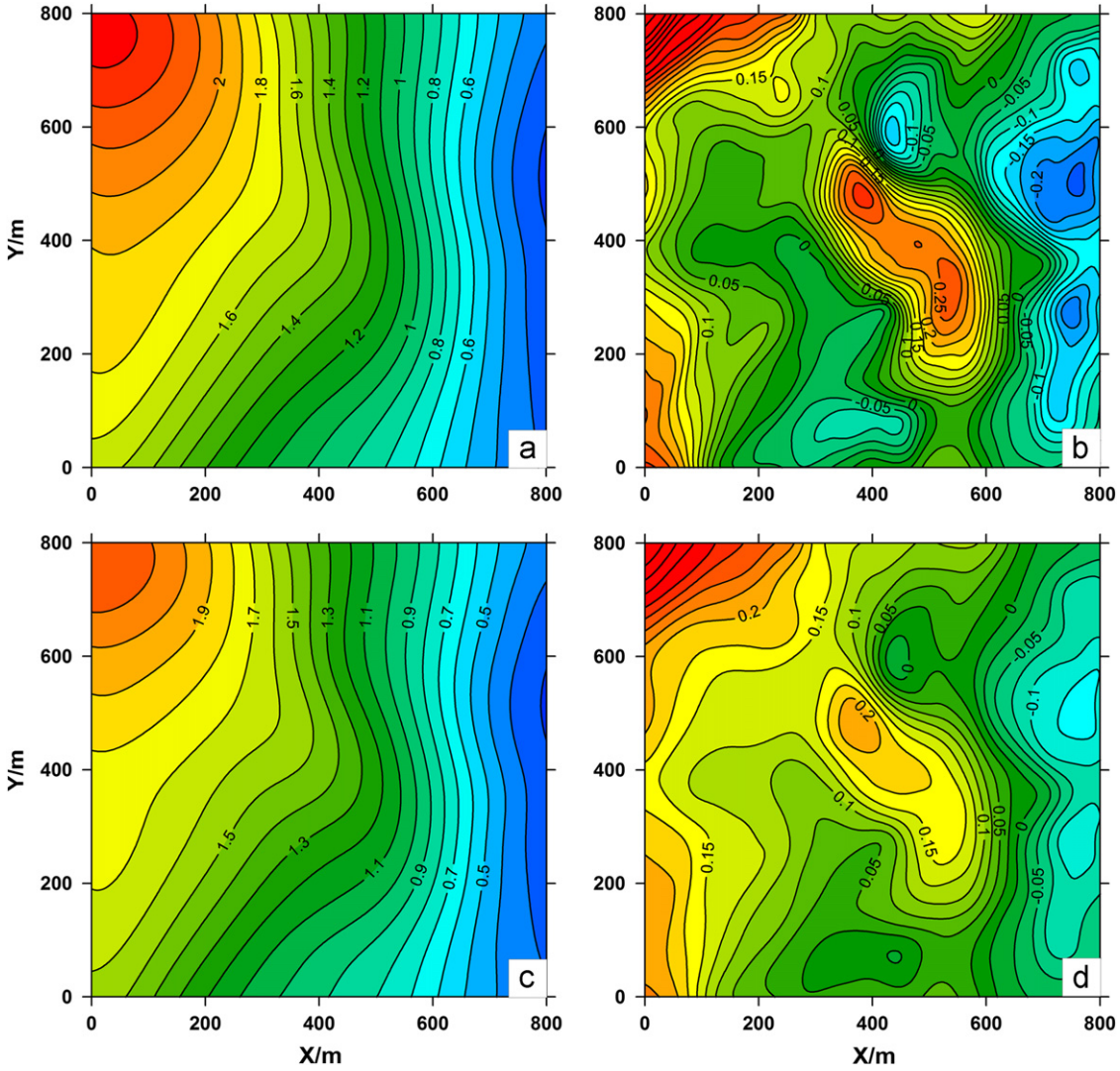


**Fig. 9.** The regional (a) and local (b) anomalies separated by using the conventional low-pass filtering, and those (c and d) of the upward continuation. The unit of gravity anomaly is mGal.

effective anomalies were slightly suppressed by the upward continuation. The separated regional anomalies of layer A were well preserved by the preferential filtering, while those of the low-pass filtering were partially suppressed and those of the upward continuation were seriously suppressed. The separated local anomalies of layers B and C by the preferential filtering contained little regional anomalies, while those of the low-pass filtering remained partially regional anomalies and those of the upward continuation preserved more regional anomalies implying an incomplete separation.

### 3.2. Test on the real data

The real Bouguer gravity anomaly data (Fig. 6) came from one magnetite area in Jilin Province, China (Chen, 1987; Zeng et al., 2008). The density difference between the magnetite and the country rocks in this area is about 1.0–1.2 g/cm$^3$, while that between the skarn and the country rocks is about 0.3–0.5 g/cm$^3$. In the case that the body of skarn or magnetite is large enough and locates relatively shallow, such a difference can produce significant gravity anomalies. The regional gravity anomalies (Fig. 6) in this area strike NNE, consistent with the regional tectonic strike. Overall, the regional anomalies decrease gradually from northwest to southeast with a nose-like local high anomaly in the center of the area. The trap portion of this local anomaly coincides well with the magnetite outcrop on the surface, while the other portions are not clear due to interference of the regional anomalies and the Quaternary cover.

We calculated the radially averaged logarithm power spectrum of the Bouguer gravity anomaly and then fit it by using piece-wise linearization (Fig. 7). In this case, we separated the radial frequency of the power spectrum into six sections, 0–0.0016 cycles/m (frequency band 1), 0.0016–0.0074 cycles/m (frequency band 2), 0.0074–0.0145 cycles/m (frequency band 3), 0.0145–0.0297 cycles/m (frequency band 4), 0.0297–0.0599 cycles/m (frequency band 5), and 0.0599–0.1 cycles/m (frequency band 6). The power spectrum of frequency band 1 was mainly related to regional anomalies, that of frequency bands 2 and 3 to local anomalies, and that of frequency bands 4–6 to high-frequency random noise. Then we used the preferential filtering method to separate the regional anomalies and the local anomalies, respectively shown in Fig. 8a and b.

In Fig. 8a, the separated regional anomalies trend in NNE with relatively higher values in the west and lower values in the east, and no local anomalies are contained. In Fig. 8b, the local high anomalies with two traps appear in the center of the area, and no obvious regional anomalies are retained, implying a fairly complete separation. The small traps nearby point (350 m, 350 m) are consistent with the magnetite outcrop on the surface, while the surface of the big trap around point (330 m, 530 m) was covered by the Quaternary terrane. We deduced that the big trap associated with iron ore of high density. The real drilling of ZK23 and ZK24 (see points in Fig. 8b) proved a certain reserve of iron ore beneath this site.

For comparison, we also did the same data test by using the conventional low-pass filtering and the upward continuation, respectively. Fig. 9a and b, respectively, shows the denoised anomalies and the separated regional anomalies by the low-pass filtering; Fig. 9c and d displays those of the upward continuation. The results show that the regional-residual anomalies separation by both methods was not complete. The local anomalies (Fig. 9b) separated by the low-pass filtering remained partially regional anomalies featured by being slightly high in the west while being low in the east, and those (Fig. 9d) of the upward continuation contained more regional anomalies that are obviously high in the west while being low in the east, implying an incomplete anomaly separation.

## 4. Conclusions

We have presented the preferential filtering method based on Green equivalent-layer concept and Wiener filter, which separates gravity anomaly without the requirement of continuation height. The principle and the procedure of the method were provided. Tests with synthetic gravity data and real gravity data show that the method is effective and produces better separation of gravity anomaly than both the conventional low-pass filtering and the upward continuation.

However, we do not consider the preferential filtering to be superior to the conventional methods mentioned in the introduction in all situations. The preferential filtering has its limitations. For instance, the method uses Green equivalent layer to approximate the anomalous source in the subsurface and assumes that the anomalies of target layers are not correlated with those of the other layers. This assumption is, however, not always appropriate in practice. It is possible for the so-called shallow sources to extend at great depth and this makes the separation difficult (Keating and Pinet, 2011). On the other hand, the spectrum of most geological features is broadband and the spectra of features located at different depths overlap so that their spectra cannot be separated completely (Telford et al., 1990).

## Acknowledgments

We thank two anonymous reviewers for their helpful comments and valuable suggestions. This work was supported by the financial support of The National Natural Science Foundation of China (40904033), The Fundamental Research Funds for the Central Universities and the SinoProbe projects (201011039).

## References

Boler, F.M., 1978. Aeromagnetic Measurements, Magnetic Source Depths, and the Curie Point Isotherm in the Vale-Owyhee, Oregon. M.S. Thesis, Oregon State University, Corvallis.
Chen, S., 1987. Gravity exploration. Geological Publishing House, Beijing, China (in Chinese).
Clarke, G.K.C., 1969. Optimum second-derivative and downward continuation filters. Geophysics 34, 424–437.
Connard, G., Couch, R., Gemperle, M., 1983. Analysis of aeromagnetic measurements from the Cascade Range in central Oregon. Geophysics 48, 376–390.
Dampney, C.N.G., 1969. The equivalent source technique. Geophysics 34, 39–53.
Fedi, M., Quarta, T., 1998. Wavelet analysis of the regional-residual and local separation of potential field anomalies. Geophysical Prospecting 46, 507–525.
Guo, L., Meng, X., Chen, Z., 2009. Preferential upward continuation and the estimation of its continuation height. In: CPS/SEG Beijing 2009 International Geophysical Conference & Exposition, Beijing, China, ID1164.
Hestenes, M.R., Stiefel, E., 1952. Methods of conjugate gradients for solving linear systems. Journal of Research of the National Bureau of Standards 49, 409–436.
Jacobsen, B.H., 1987. A case for upward continuation as a standard separation filter for potential field maps. Geophysics 52 (8), 1138–1148.
Keating, P., Pinet, N., 2011. Use of non-linear filtering for the regional-residual separation of potential field data. Journal of Applied Geophysics 19, 315–322.
Meng, X., Guo, L., et al., 2009. A method for gravity anomaly separation based on preferential continuation and its application. Applied Geophysics 6 (3), 217–225.
Naidu, P., 1968. Spectrum of the potential field due to randomly distributed sources. Geophysics 33, 337–345.
Nettleton, L.L., 1954. Regionals, residuals and structures. Geophysics 19 (1), 1–22.
Pawlowski, R.S., Hansen, R.O., 1990. Gravity anomaly separation by Wiener filtering. Geophysics 59 (1), 539–548.
Pawlowski, R.S., 1994. Green's equivalent-layer concept in gravity band-pass filter design. Geophysics 55 (5), 69–76.
Pawlowski, R.S., 1995. Preferential continuation for potential-field anomaly enhancement. Geophysics 60 (2), 390–398.

Spector, A., Grant, F.S., 1970. Statistical models for interpreting aeromagnetic data. Geophysics 35 (2), 293–302.
Telford, W.M., Geldart, L.P., et al., 1990. Applied Geophysics. Cambridge University Press, Cambridge, UK.
Wiener, N., 1949. Extrapolation, interpolation, and smoothing of stationary time series. John Wiley & Sons Inc, USA.
Xu, D., Zeng, H., 2000. Preferential continuation and its application to Bouguer gravity anomaly in China. Geoscience 14, 215–222 (in Chinese).
Zeng, H., Xu, D., Tan, H., 2008. A model study for estimating optimum upward-continuation height for gravity separation with application to a Bouguer gravity anomaly over a mineral deposit, Jilin province, northeast China. Geophysics 72 (4), I45–I50.